Proceedings of ASME Turbo Expo 2011
GT2011
June 6-10, 2011, Vancouver, British Columbia, Canada

GT2011-46863

FAILURE INVESTIGATION OF 1ST STAGE BUCKETS FROM FRAME 3002, 10 MW GAS TURBINE UNIT

Girish M. Shejale*
Quality Control Department
Masaood John Brown
PO Box-11931, Dubai
United Arab Emirates
Phone: +971-4-8836319
Email: gshejale@mjbi.com

David Ross
Engineering Department
Masaood John Brown
PO Box-11931, Dubai
United Arab Emirates
Phone: +971-4-8836319
Email: dross@mjbi.com

ABSTRACT
The 1st stage buckets in Frame 3002, 10 MW industrial gas turbine experienced premature failures. The buckets failed unexpectedly much earlier than the designed bucket life. Bucket material is Inconel 738, with platinum-aluminized coating on the surface. Failure investigation of the buckets was performed to know the root cause of the failure. The failure investigation primarily comprised of metallurgical investigation. The results of the metallurgical investigation were co-related with the unit operational history.

This paper provides an overview of 1st stage buckets investigation. The metallurgical investigation performed concluded prime failure mechanism due to high carbon content of bucket material and improper heat treatment. The bucket coating was initially damaged during the first loading and fracture occurred due to grain boundary embrittlement in short span of service. The metallurgical tests performed included Visual inspection, Scanning Electron Microscopy (SEM), Energy Dispersive Analysis of X-ray (EDS), Chemical analysis, Tensile test and Hardness survey. The test results, discussions and conclusions are presented in this paper.

* Author of correspondence

KEYWORDS: buckets, carbides, embrittlement, failure investigation, gamma prime, heat treatment, microstructure and oxidation.

1. INTRODUCTION
In a gas turbine, Stage 1 buckets experience most severe combination of temperature, stress and environment. The material of first stage buckets in gas turbine is nickel-based alloy. Inconel 738 is notable as being one of a very useful class of superalloys that has an outstanding combination of elevated temperature strength and high temperature corrosion. Further, to protect the 1st stage bucket surface from high temperature oxidation and hot corrosion platinum-aluminide coating is applied [1]. Failure of the 1st stage buckets will have a significant impact on the availability of the gas turbine engines, thus leading to high production losses. The common modes of failure of buckets is creep, fatigue (low cycle and high cycle); corrosion/oxidation; foreign object damage; excessive strain/distortion; wear and fretting [2]. Failure investigation is necessary to know the root cause of failure. Through failure investigation the root cause of failure can be identified and recurrence of similar type of failures can be eliminated.

The present work reports the failure investigation of a 1st stage bucket from Frame 3002, 10MW gas turbine unit. Several buckets had experienced failure in service. Metallurgical investigation was performed on the selected failed buckets with combination of tests. This paper provides an overview of the metallurgical investigation which includes test results, discussions and conclusions.

2. BACKGROUND

Several 1st stage buckets from Frame 3002, 10MW gas turbine unit experienced premature failure while in service. Unit model number is M3142. The fuel used was natural gas. Firing temperature is 943 ^{0}C and exhaust temperature is 526 ^{0}C. This firing temperature is associated with first stage buckets. The turbine speed is 7107 RPM. The turbine was in continuous operation and failure of 1st stage buckets occurred in service. The turbine had accumulated total 66,000 running hours. Prior to failure the 1st stage buckets were new and in service for an estimated 15 to 20 hours and had been installed during a major upgrade including the turbine control system. The buckets failed during the first start-up after the up gradation.The material of the 1st stage buckets as per specification is Inconel 738LC. The buckets are hollow and un-cooled. There were no abnormalities in engine operation prior to the occurrence of failure. The thrust bearing temperature and condition of lubricating oil system was normal. The vibration monitoring probes were running normal. Alarm trips and safety devices were quite intact. There were no repairs and modifications of any kind carried out on the engine. The schematic view showing the failure location of 1st stage buckets is shown in Figure 1. The combustion cans when removed from the unit visually displayed discoloration as shown in Figure 2. The transition piece and fuel nozzle also exhibited visual signs of discoloration as shown in Figure 3. The combustion cans and transition pieces were installed along with the first stage buckets.

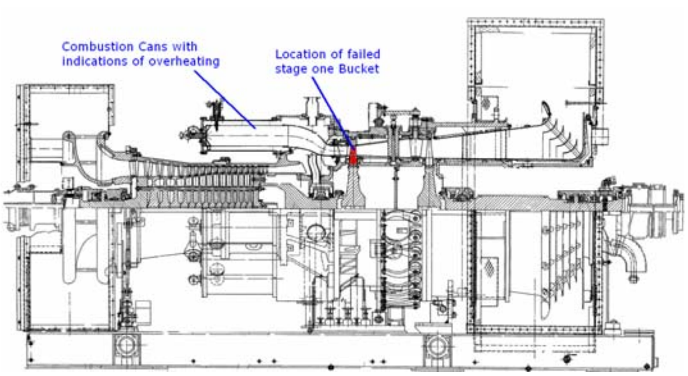

Figure 1: Schematic view of the turbine section showing the location of failed 1st stage buckets.

Figure 2: Photograph of combustion cans showing discoloration after 15 to 20 hours of service.

Figure 3: Photograph of transition piece and fuel nozzle showing discoloration.

3. EXPERIMENTAL WORK

Two failed buckets were received from site. Buckets were identified as bucket 1 and 2. The visual fracture appearance of both the buckets was similar in nature. Bucket 2 was selected for a detailed metallurgical testing. The tests performed were Visual examination, Chemical analysis, Scanning Electron Microscopy (SEM), Energy Dispersive Analysis of X-ray (EDS), Microexamination, Tensile test and Micro hardness survey.

3.1. Visual Examination:

The failed buckets in the as received condition are shown in Figure 4. Fracture surface of both the buckets is similar in appearance with uneven contours and a smooth zone. The failure appears to be in the upper portion of airfoil. Buckets are hollow from inside and un-cooled. The fracture surface is oblique to blade axis. Fracture surface appears to be grayish black in color and shows signs of oxidation. Discoloration is observed near the fracture region on the bucket surfaces. This is observed on both the concave and convex surfaces. The root portion is un- affected and is sound. Root portion did not show any deformation or discoloration. The fracture surfaces are shown in Figures 5 and 6.

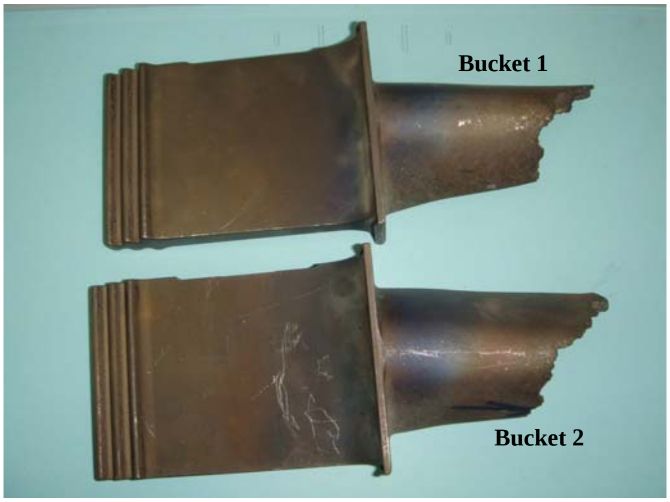

Figure 4: Photograph of the buckets in the as received condition.

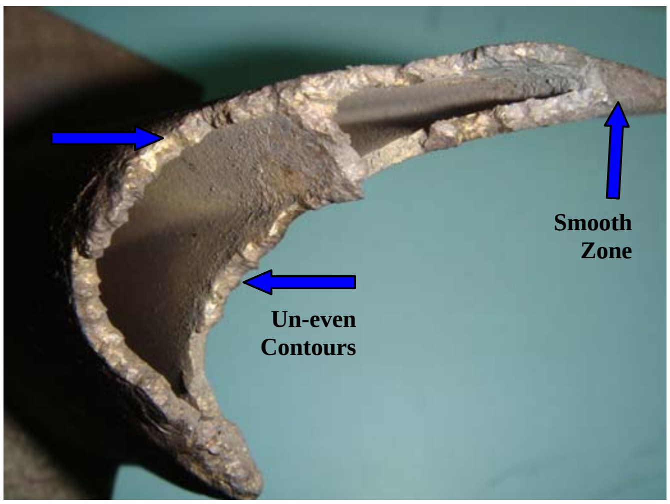

Figure 5: Photograph of Bucket 1 showing the fracture surface; un-even contours and a smooth zone is evident.

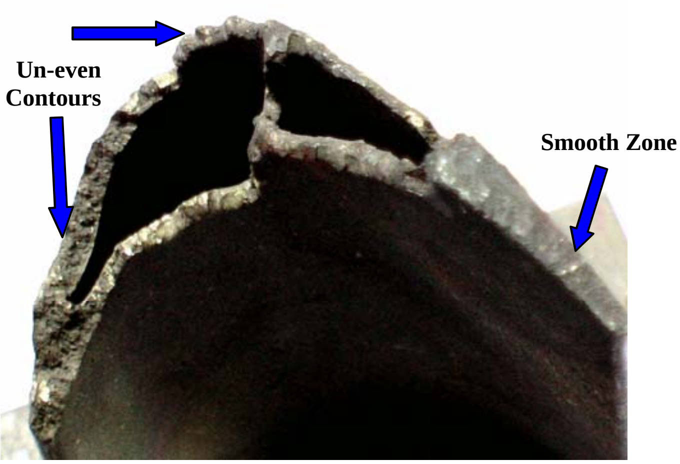

Figure 6: Photograph of Bucket 2 showing the fracture surface; un-even contours and smooth zone is evident.

3.2. Chemical Analysis:

The chemical analysis was performed using optical emission spectrometer on bucket 2 at the root area. The analysis is given in Table 1. The high carbon content of 0.15 percent along with other alloying elements indicates that the material grade of bucket is Inconel 738. This does not comply with the original material of construction Inconel 738LC.

Table 1. Chemical analysis result of bucket material.

Elements	Percentage, %
Carbon	0.15
Chromium	15.97
Nickel	Balance
Molybdenum	1.94
Aluminium	3.38
Iron	0.15
Niobium	1.04
Titanium	3.36
Cobalt	8.67
Tungsten	2.61
Tantalum	1.92
Manganese	0.008
Sulfur	0.005
Boron	0.0051
Zirconium	0.062

3.3. Scanning Electron Microscopy (Fracture Surface):

SEM analysis was performed on sectioned fracture surface of bucket 2 shown in Figure 6. The fracture section was ultrasonically cleaned prior to SEM examination. The fracture surface with un-even contours exhibits gross plastic deformation. Secondary cracks are evident at the un-even contour zone. Cracks appear to be intergranular. A mixed mode of ductile and brittle fracture is evident [3]. Presence of oxidized scale is evident, which is significant in the smooth fracture zone. The SEM photographs are presented in Figures 7 to 10.

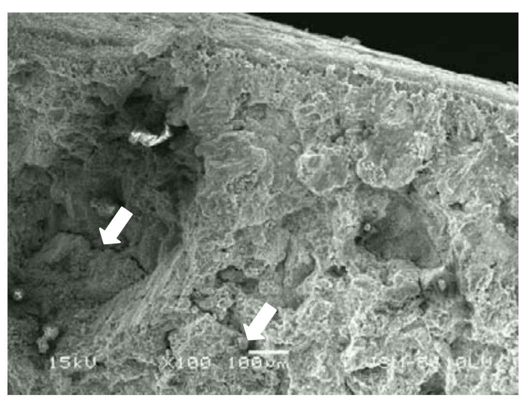

Figure 7: SEM photograph of fracture surface at un-even (rough zone) area showing ductile mode; secondary cracks are evident (arrows); Original Magnification – 100x

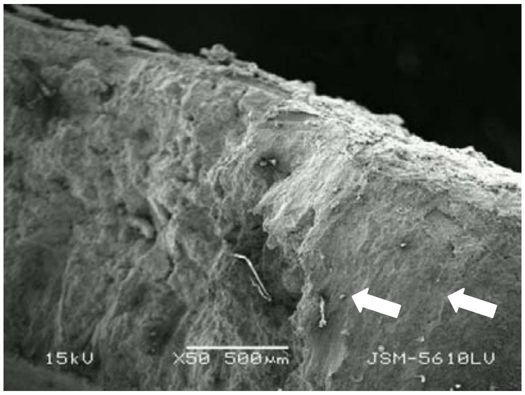

Figure 8: SEM photograph at fracture transition zone; showing fracture progression; mixed mode of fracture is evident; Original Magnification – 50x

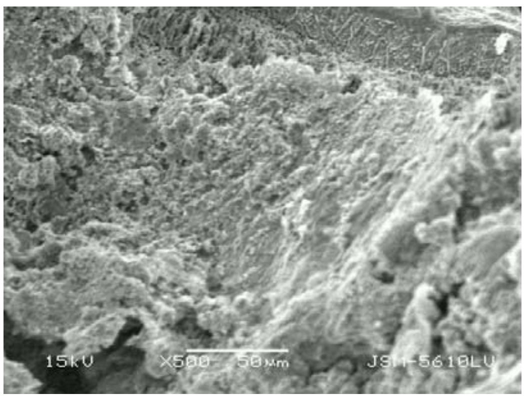

Figure 9: SEM photograph near to the fracture transition zone; ductile mode along with oxidized scale is observed; Original Magnification – 500x

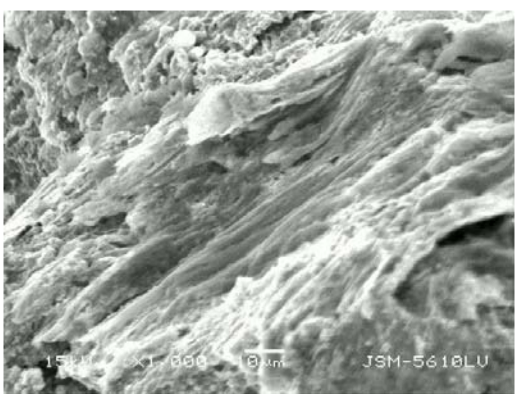

Figure 10: SEM photograph towards the smooth fracture zone; presence of oxidized scale is observed; Original Magnification – 1000x

3.4. Energy Dispersive Analysis of X-Ray (EDS):

EDS was performed on the fracture surface at several locations. The representative EDS spectrum at the outer fracture edge is shown in Figure 11 and the elemental quantification is given in Table 2.

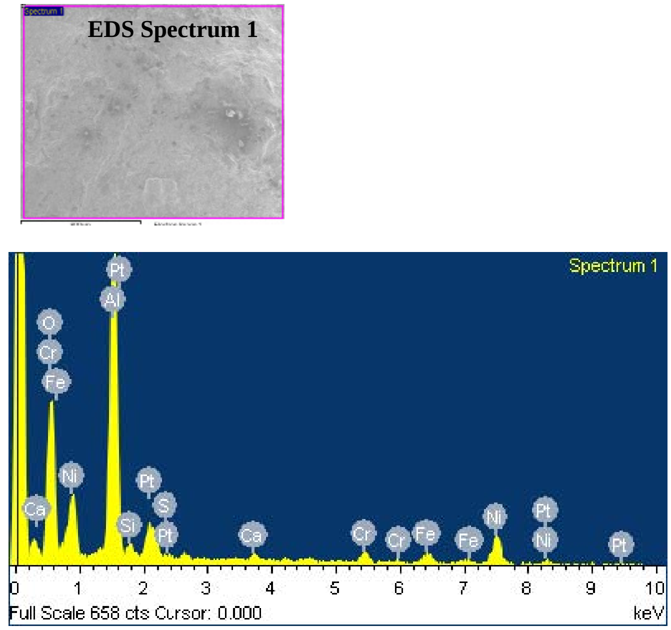

Figure 11: EDS representative spectrum performed on fracture surface towards the edge.

Table 2. EDS representative elemental analysis for Figure 11.

Elements	Percentage
Oxygen	33.04
Aluminum	26.90
Silicon	1.48
Sulfur	0.26
Calcium	1.06
Chromium	3.36
Iron	4.44
Nickel	20.63
Platinum	8.83

The analysis reveals high amount of aluminum and platinum indicating presence of platinum-aluminized coating on the bucket surface. Considerable amount of oxygen is observed. Presence of sulfur is considered as detrimental element for hot corrosion [4].

3.5. Macrostructure Examination:

The bucket 2 was sectioned in transverse/ longitudinal direction to examine the macrostructure. The section was polished and then etched with acid. This was performed to view the grain structure morphology. The section displays typical cast structure. Coarse grains are observed in thick section and fine grains were observed at thin section. The grain morphology as such did not display any abnormality. Macroetched section is shown in Figure 12.

Figure 12: Photograph of macroetched section; grain pattern indicates a cast structure.

3.6. Microexamination (Light Optical Microscope):

Microsections were taken on bucket 2 at several locations which included fracture at origin towards the leading edge, longitudinal and transverse sections away from the fracture. Microstructural examination near the fracture area and away from the fracture area are discussed and presented. Microstructure at the fracture surface exhibits secondary cracks. Several cracks are evident in the coating at the fracture area and away from fracture area. Cracks originated from coating have propagated further in the bucket material. Cracks in bucket material are intergranular and appears to be branched at some locations. Porosity is evident at the fracture area [5]. The general microstructure of bucket material displays an austenitic matrix along with dispersed carbides. Microstructure consists of MC and $M_{23}C_6$ carbides. Excessive carbide precipitation along the grain boundaries is evident near to and away from the fracture surface. Root area microstructure did not display significant carbide precipitation. Photomicrographs are presented in Figures 13 to 22.

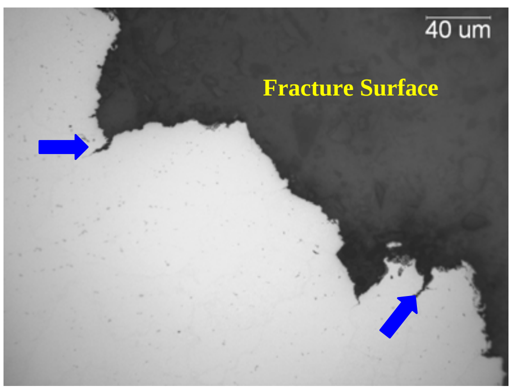

Figure 13: Photomicrograph of section near fracture; secondary cracks are evident (arrows); Un-etched.

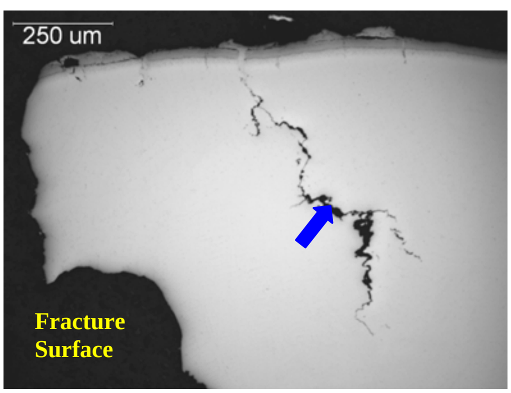

Figure 14: Photomicrograph of section near fracture; coating appears to be damaged and exhibits cracks; branched cracking originating from coating is evident (arrow); Un-etched.

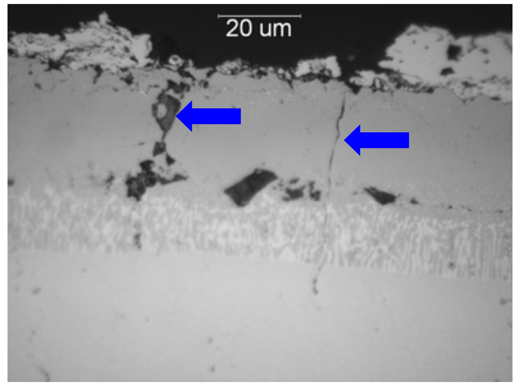

Figure 15: Photomicrograph of the section near the fracture surface; coating display cracks (arrows); Un-etched.

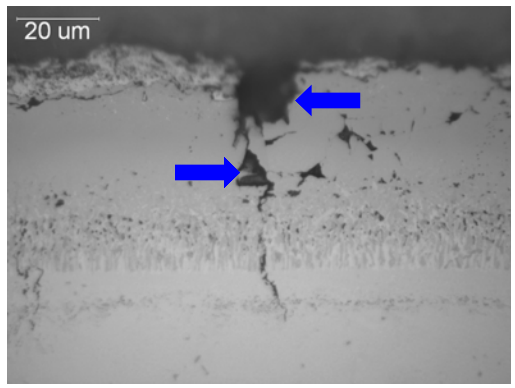

Figure 16: Photomicrograph of the section away from fracture surface; note the crack along with oxidation (arrows); Un-etched.

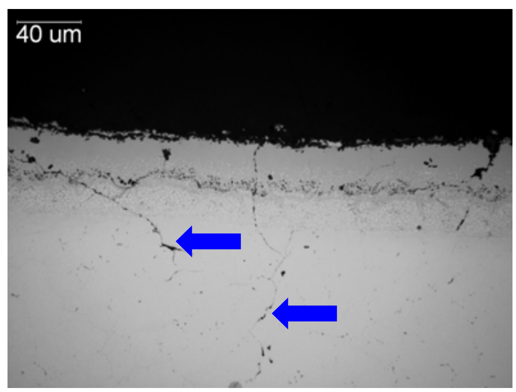

Figure 17: Photomicrograph of the section away from fracture surface at another location; coating displays cracks (arrows); Un-etched.

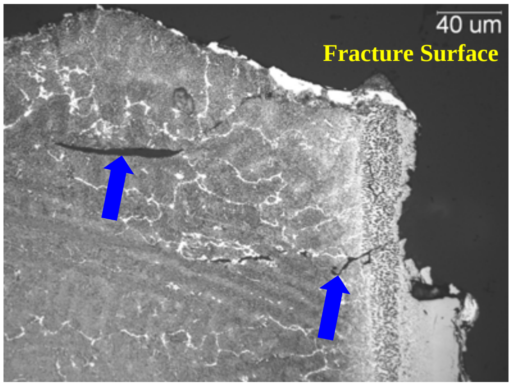

Figure 18: Photomicrograph of section at fracture surface; cracks initiating from coating and propagating in bucket material are evident (arrows); Etched.

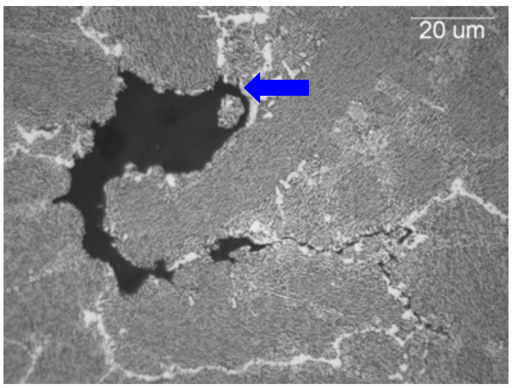

Figure 19: Photomicrograph of section near to fracture surface; porosity is observed (arrow); Etched.

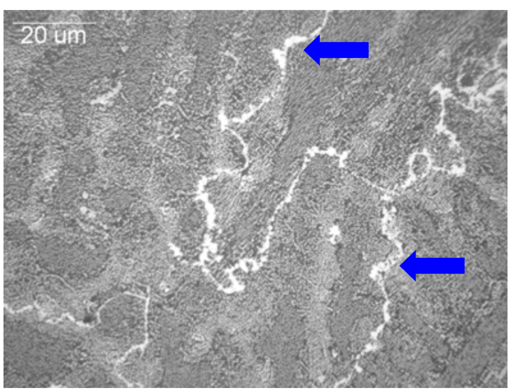

Figure 20: Photomicrograph of general microstructure at the fracture area; note the carbide precipitation along the grain boundary (arrows); Etched.

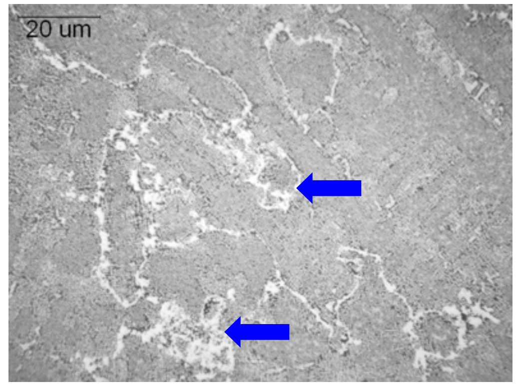

Figure 21: Photomicrograph of general microstructure at the mid-section area of bucket (away from fracture); excessive carbide precipitation is evident along the grain boundary (arrows); Etched.

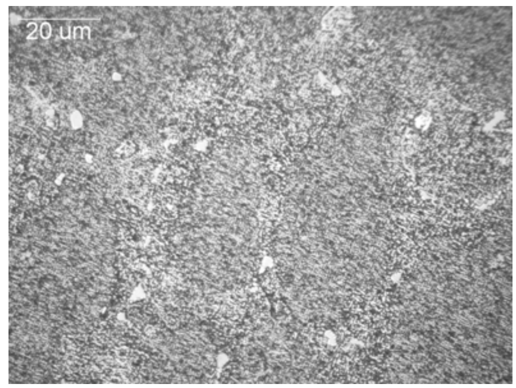

Figure 22: Photomicrograph of general microstructure at the root area of bucket; Etched.

3.7. Energy Dispersive Analysis of X-Ray (EDS) of Carbides:

EDS was performed on the carbides at the top side section (near fracture area) and root section of the bucket. The EDS spectrum locations on carbides are indicated as X in Figure 23. The representative EDS spectrums are shown in Figures 24 and 25 and the elemental quantification is given in Table 3.

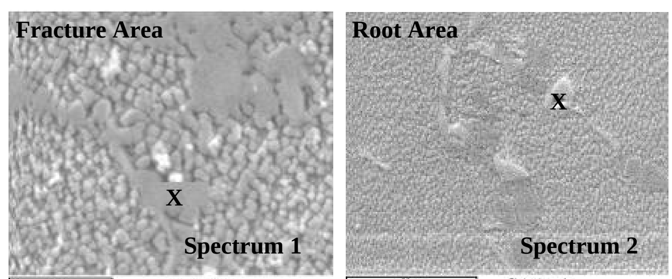

Figure 23: EDS representative spectrum performed on carbides at the fracture area and root area.

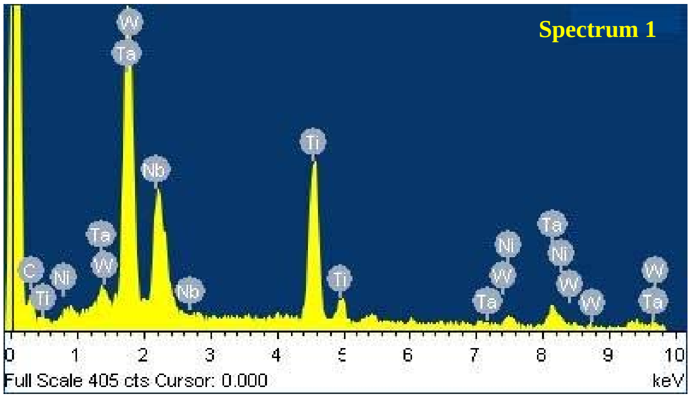

Figure 24: EDS representative spectrum 1 performed near fracture area as shown in Figure 23.

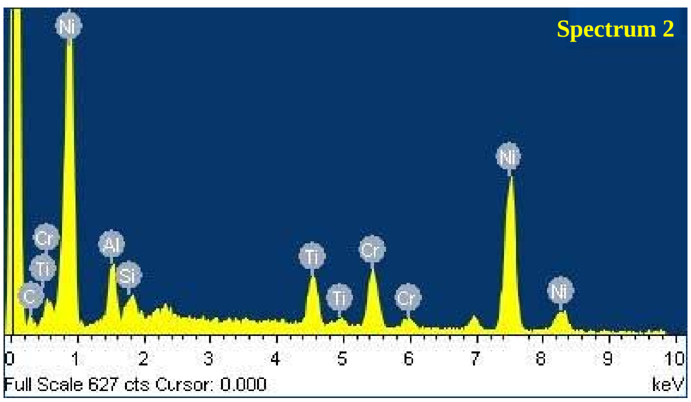

Figure 25: EDS representative spectrum 2 performed at the root area as shown in Figure 23.

Table 3. EDS representative elemental analysis for Figures 24 and 25.

Elements	Fracture Area Spectrum 1	Root Area Spectrum 2
Carbon	4.10	9.31
Titanium	6.51	22.11
Nickel	73.12	5.38
Aluminum	4.52	-
Silicon	1.26	-
Chromium	10.49	-
Niobium		17.88
Tungsten		8.25
Tantalum		37.06

The carbides at fracture area exhibits presence of Al, Cr, Ni, and Ti. This appears to be $M_{23}C_6$ type carbide. Carbide at the root area is rich in Ta, Ti and Nb and appears to be MC type carbide.

3.8. Microexamination (Scanning Electron Microscope):

SEM analysis was performed to check the gamma prime morphology at different areas of the bucket. Gamma prime morphology was examined at the fracture area (top area), middle area and at the root area of the bucket 2. Gamma prime is geometrically close-packed phase and generally is Ni_3Al or $Ni_3(Al,Ti)$, although considerable elemental substitution occurs [6]. Coarsening and coalescence of gamma prime is observed at the fracture area, which are round in shape. Middle area exhibits comparatively finer (medium to fine) gamma prime than the fracture area. They are rounded and little cuboidal in shape. Gamma prime at the root area was medium to fine, with rounded and cuboidal shape. This is not considered to be typical after a proper heat treatment. Primary and secondary precipitates are observed at the middle area and root area. Volume fraction of the gamma prime was measured. The volume fraction of gamma prime is 41.82% at the fracture area, 37.42% at the middle area and 33.73% at the root area. In general, the fracture area exhibits the highest gamma prime volume fraction as compared to the middle area and root area. SEM micrographs are presented in Figures 26 to 28.

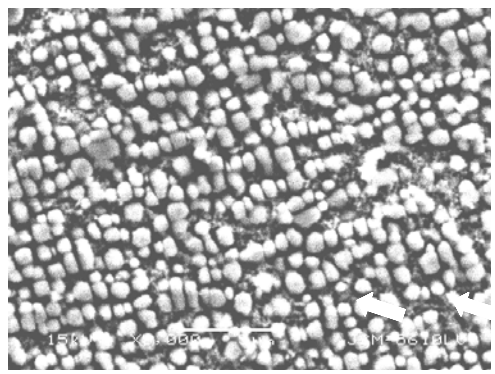

Figure 26: SEM photograph at Location A showing coarse gamma prime; Volume fraction 41.82%, Original Magnification – 5000x

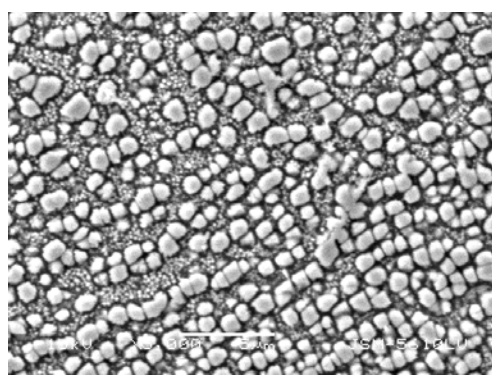

Figure 27: SEM photograph at Location B showing medium coarse rounded and cuboidal gamma prime; Volume fraction 37.42%, Original Magnification – 5000x

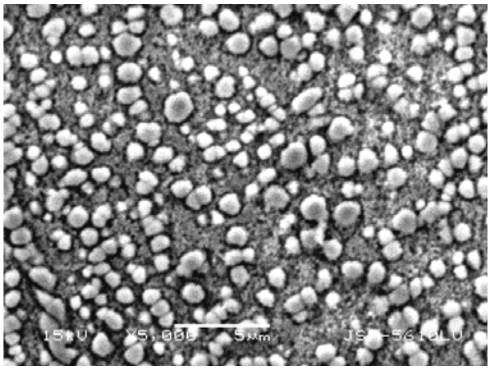

Figure 28: SEM photograph at Location C showing medium to fine gamma prime; Volume fraction 33.73%, Original Magnification – 5000x

3.9. Mechanical Tests:

Tensile test was performed at the section taken from root area of bucket a shown in Figure 29. This test was performed at room temperature. Tensile test results are presented in Table 4.

Figure 29: Photograph of bucket showing the tensile test location towards the root area.

Table 4. Tensile test results of bucket at root area.

Parameter	Measured Value
Temperature	Room Temperature
Yield Stress (N/ mm^2)	788
Ultimate Tensile Strength (N/ mm^2)	852
Elongation (%)	4.80

In general the tensile test result values were found to be acceptable for the bucket material. There is no data available to compare the tensile test results with the Inconel 738 bucket material.

3.10. Micro-hardness Test:

Micro-hardness test was performed on the microsections at the fracture surface, away from fracture surface and root area. The results are tabulated in Table 5.

Table 5. Micro-hardness test results of bucket sections.

Location	Hardness Values (HV) 300 gms load	Average Value (HV)
Fracture Area	461, 456, 451, 447	454
Away from fracture area	388, 392, 390, 386	389
Root Area	392, 390, 382, 388	388

The hardness values at the fracture area are on the higher side as compared to the hardness values away from fracture and at root area. The hardness values at the root area, which is considered to be un-affected area, are in acceptable range for Inconel 738 bucket material.

4. DISCUSSION

Visual examination reveals that fracture surface is oblique to the bucket axis. Fracture has uneven contours and both the received buckets have similar type of fracture appearance. The chemical analysis results are not consistent with Inconel 738 LC material grade. Macrostructure examination suggests that grain morphology is typical of a cast bucket. SEM fracture morphology indicates failure modes associated with intergranular type of fracture. Damage to platinum-aluminide coating is also evident along with oxidation. Microstructural examination reveals damage to coating with cracks at the fracture area and away from fracture area. The coating cracks have occurred during the first start up since the buckets were in operation. Cracks have initiated in the coating and further propagated in the bucket material. Microstructure at the fracture surface indicates continuous carbide network along the grain boundaries. MC carbides and $M_{23}C_6$ carbides are observed. At high temperatures in service, MC carbides dissolve into the matrix and forms $M_{23}C_6$ carbides enveloped in gamma prime. EDS analysis reveals that fracture area primarily consists of $M_{23}C_6$ carbides. The presence of heavy or continuous network of grain boundary $M_{23}C_6$ carbides at airfoil section can facilitate grain boundary sliding and crack propagation by boundary-matrix decohesion. These carbides decrease the grain boundary strengthening mechanism and can contribute to brittle fracture behaviour [7]. The carbide analyzed at the root area is of MC type, which is rich in tantalum. The amount of MC or $M_{23}C_6$ carbides will depend on the carbon content in the bucket material. The bucket material is Inconel 738 with observed carbon content of 0.15 percent. This carbon content is considered to be high and have contributed in formation of MC or $M_{23}C_6$ carbides. The probability of such carbide formation tendency will be less in Inconel 738LC material due to the low carbon content.

Presence of porosity is evident at the fracture surface. Coarsening and coalescence of gamma prime is evident at the fracture area. This is more prominent at the fracture area and the intensity decreases moving away from the fracture area. Coarse gamma prime and coalescence indicates some evidence of overheating, which is not considered to be significant.

Coarsening of gamma prime is closely related to losses in tensile strength and creep strength [8]. The root area did not display indications of overheating as evident by the observed gamma prime morphology along with secondary precipitates. The gamma prime structure at root area is not typical for a normal heat treated Inconel 738 alloy. Volume fraction of gamma prime is highest at fracture area as compared to the mid-area and root area of the bucket. In general, volume fraction of gamma prime increases with addition of aluminum and titanium. A difference in gamma prime volume fraction could be on account of slight local variation in chemical composition.

EDS at the fracture surface revealed presence of sulphur at some locations, but did not reveal presence of any sodium or vanadium. With this there is no possibility of hot corrosion attack on the bucket surface. The presence of high oxygen along with iron suggests oxidation at high temperatures. The aluminide/MCrAlY coating provides oxidation resistance at high temperature and protects the base material. Oxidation resistance is attributed to β-aluminide phase which forms a protective layer, which slows down the oxidation process. Coating failures can occur due to depletion of β-aluminide phase or thermal-mechanical coating cracks [9]. The possibility of FOD (Foreign Object Damage) or DOD (Domestic Object Damage) mechanism was eliminated as this would have been evident on the upstream parts such as first stage nozzles and transition pieces.

Based on the evidences the sequence and mode of failure can be explained. The Inconel 738 buckets have a high carbon content due to which network of $M_{23}C_6$ carbides along the grain boundaries is formed. There is an evidence of $M_{23}C_6$ carbide network at the fracture surface along the grain boundaries. Presence of Aluminum indicates there is a possibility of Ni_3Al type carbides in this area. The $M_{23}C_6$ carbide network is considered to embrittle the grain boundaries in short span of service duration. The acting in-service stress possibly have resulted in stress related grain boundary oxidation and cracking. This cracking and the cracks in the coating have further propagated in the substrate (bucket material) has resulted in fracture of the bucket at operational temperatures. Primarily the crack initiation and propagation occurred at the trailing edge of the bucket. The newly installed buckets were in service for 15 to 20 hours prior to failure. In such a short span of time the excessive carbide precipitation at airfoil area of the bucket is not considered to be normal. The gamma prime morphology at the root area and the observed carbide precipitation at the fracture area suggest improper heat treatment of the buckets. Further, the visual signs of discoloration on the combustion cans, transition piece and fuel nozzle in a span of 15 to 20 hours suggest possibility of high operational temperatures in the unit. There is a possibility that the high temperatures in service may have contributed to the fracture of buckets.

The metallurgical investigation of the buckets suggests that the predominant damage mechanism is grain boundary embrittlement and cracking due to high carbon content associated with improper heat treatment. High temperatures in service could have been a contributing factor. The records of operational temperatures of the unit are not available.

5. CONCLUSION

The metallurgical failure investigation of the 1st Stage bucket concludes the following:

1. The premature failure of buckets is primarily attributed to high carbon content in bucket material and improper heat treatment. There is a possibility that high temperatures in service may also have contributed to the failure.
2. It is envisaged that stress related grain boundary oxidation and cracking could be one of the prime contributing factor, which has resulted in fracture.
3. The cracking of platinum-aluminide coating has occurred during the first start up after installing the buckets.
4. The bucket material is high in carbon and not consistent with specified material Inconel 738LC.
5. Microstructural evidence of precipitated $M_{23}C_6$ carbides at airfoil area and the gamma prime morphology at the root area suggests incorrect heat treatment.
6. Control system needs to be set correctly in accordance to the OEM manual to prevent un-expected temperature rise in the unit.
7. Recurrence of such failures can be prevented by ensuring installation of specified bucket material (Inconel 738LC) and a proper heat treatment.

6. REFERENCES

[1] Schilke, P.W. and Schenectady, N.Y., 2004, “Advanced Gas Turbine Materials and Coatings Gas Turbine Repair Technology”, GE Energy, GER 3569G, pp. 12.

[2] Pallos, K.J., *“Gas Turbine Repair Technology”* 2001, GER 3957B, Atlanta, GA, pp. 7.

[3] ASM Handbook, 2002, Failure Analysis and Prevention ASM International, Volume 11, pp. 522-524.

[4] David Hendrix., 1998, “Hot Corrosion Failure of a 25 MW Land-based Gas Turbine in a Marine Environment”, *NACE Proceedings of Corrosion98”,* Paper No. 203, pp. 4-5.

[5] Cesar Roberto de Farias Azevedo, Marcelo Ferreira Moreira, Eduardo Hipperet Jr., 2001, *Nickel Superalloy (Inconel 713C)*, IPT Sao Paulo, pp. 24.

[6] ASM Handbook, 2004, *Metallography and Microstructure*, ASM International, Volume 9, pp. 834-835.

[7] Joseph, L., Paul, L., Douglas, N., Tiberius, P., Stephanie, S., 2009, "Practical Experience with the Development of Superalloy Rejuvenation", *ASME Turboexpo Gas Turbine Technical Congress and Exposition",* Orlando, Florida, USA, Paper No. GT2009-59444, pp. 4-5.

[8] Viswanathan, R., 2006, *Damage Mechanisms and Life Assessment of High-Temperature Components*, ASM International, pp. 454, Chap. 9.

[9]Lowden, P., Turcott, S., Perrin, M., Hastie, S., Oct 2009, "The Role of Metallurgical Analysis in Gas Turbine Maintenance" *Proceedings of 18th Symposium of the Industrial Application of Gas Turbines Committee,* Banff, Alberta, Canada, pp. 5-6.